Composition dependent properties of graphene (oxide)-alginate biopolymer nanocomposites

Vilcinskas, Karolis; Jansen, Kaspar M B; Mulder, Fokko M.; Picken, Stephen J.; Koper, Ger J M

DOI
10.1002/pc.24223

Publication date
2016

Document Version
Accepted author manuscript

Published in
Polymer Composites

Accepted Author Manuscript of http://dx.doi.org/10.1002/pc.24223 (Wiley)

Composition dependent properties of graphene (oxide)-alginate biopolymer nanocomposites

Karolis Vilcinskas[†], Kaspar M.B. Jansen[‡], Fokko M. Mulder[†], Stephen J. Picken[†], and Ger J. M. Koper*[†]

[†] Department of Chemical Engineering, Delft University of Technology, Julianalaan 136, 2628 BL Delft, The Netherlands

[‡] Faculty of Industrial Design Engineering, Delft University of Technology, Landbergstraat 15, 2628 CE Delft, The Netherlands

Corresponding author:

*E-mail G.J.M.Koper@tudelft.nl; Tel +31 15 27 88218

Abstract

We report on the thermal, electrical and mechanical properties of alginate biopolymer nanocomposites prepared by solution casting with various amounts of graphene oxide (GO) or reduced graphene oxide (rGO). Our data shows that the thermal stability of alginate nanocomposites can be improved by the introduction of cross-linking through divalent metal cations, albeit that under these conditions little influence by the amount of rGO remains. On the other hand, the electrical conductivity of divalent metal ion cross-linked-rGO improves approximately 10 orders of magnitude with increasing weight fraction of rGO, whereas it declines for Sodium alginate-GO composites. In addition, storage moduli and glass to rubber transition temperatures show strong composition dependence as a consequence of complex interactions of the ions with both polymer and filler. We propose a mechanical model that allows for the accurate prediction of reinforcement by GO sheets in Sodium alginate-GO composites taking into account the orientational order of the sheets. Creep tests reveal the complex nature of multiple stress relaxation mechanisms in the nanocomposites although the stretched exponential Burgers' model accurately describes short time creep compliance.

1. Introduction

Inclusion of filler in polymer matrices yields composite materials with enhanced properties, such as improved electrical and/or thermal conductivity [1], better mechanical properties [2] or reduced gas permeation [3]. Carbonaceous nanofillers, like carbon black [4], carbon nanotubes [5], as well as graphene oxide and graphene [6], are amongst the most often used additives in designing composite materials with enriched properties. However, in order to achieve the desired improvement of the above-mentioned properties, it is crucial to ensure favorable interactions between filler and polymer phase [7]. Furthermore, it is also essential to consider other aspects such as filler functionalization, evolution of filler structure in a polymer matrix, interfacial effects and to obtain detailed structural information of composites [8].

Hydrocarbons, such as polystyrene or polypropylene, are often used for the preparation of graphene-polymer composites, however it requires functionalization of the graphene sheets in order to improve processability and reduce its propensity to agglomerate which usually compromises the optimal enhancement of properties. [9]. Recently several authors [10] have investigated the properties of bio-based polymer composites, namely Sodium alginate – graphene oxide composites. Alginates are naturally occurring copolymers comprised of alternating guluronic and mannuronic acid units, that form physical cross-links with divalent metal ions [11], and have been extensively used in the food industry as well as for pharmaceutical and medical applications [12]. Water-soluble Sodium alginate and hydrophilic graphene oxide (GO) offer a great advantage to the production of composites since both materials can be readily processed in aqueous medium. Upon drying of the composite sample, the abundance of hydroxyl groups on the Sodium alginate chains participates in the formation of the hydrogen-bonding network with carbonyl and/or epoxy groups on GO sheets [10b]. The resulting composites have shown to possess higher thermal stability [10a], increased Young's

modulus [10a, 10b] and improved creep resistance [10b]. On the other hand, divalent metal ion cross-linked alginate films have useful properties, such as insolubility in water, and, as has been reported for calcium alginate films, high storage modulus value and moderate glass transition temperature [13]. However, no attempts have been made to examine the properties of divalent metal ion cross-linked alginate-reduced graphene oxide (rGO) composites and to study the interactions between the polymer, filler and metal ions. Furthermore, to our knowledge, no studies have so far been reported to predict the reinforcing effect of GO sheets in the Sodium alginate matrix, and to model creep behavior of alginate composites of various compositions.

In this study, we set out to explore the thermal, electrical and mechanical properties of alkali earth metal ion cross-linked alginate-rGO composites, and to compare their properties to that of Sodium alginate-GO composites. In addition, we also consider composition-structure-properties aspects of the composites.

2. Materials and methods

2.1. Sample preparation

Sodium alginate salt (Protanal® RF 6650) was kindly provided by FMC Biopolymer. To prepare 1 wt% aqueous polymer solution, 1 gram of Sodium alginate (Na Alg) salt was dissolved in 99 grams demineralized water, containing 0.4 grams of glycerol (99+ Pure, Acros Organics) under vigorous stirring until a homogenous solution was attained.

Graphene oxide (GO) was prepared via Kovtyiukhova's method [14]. Composite films with various weight fractions of GO were prepared by drop-wise addition of aqueous GO dispersion into a 1 wt% Sodium alginate solution and continuous stirring until a homogenous mixture was attained. The mixture then was poured into a Petri dish and dried under vacuum at 50 °C overnight (about 15 h).

Subsequently, the thus obtained free-standing water-soluble Sodium alginate/GO (Na-Alg/GO) composite films of ~30 µm in thickness were cut into strips of about 30x3 mm^2 and immersed into a 5 wt% $CaCl_2$ (Sigma Aldrich) or a 5 wt% $BaCl_2$:$2H_2O$ (Riedel-de Haën) solution for 20 min to obtain alkaline earth metal cross-linked alginate composite films. The excess salt was removed using copious amounts of demineralized water. The samples were dried under vacuum at 50 °C. Note that, without the cross-linking salt, the Na-Alg/GO films readily dissolve in water since they are hydrophilic, whereas the cross-linked films are water-insoluble and form a swollen gel.

Finally, the reduced graphene oxide (rGO)/alginate composite films were prepared by immersing the water-insoluble alkaline earth metal cross-linked alginate/GO composite films, as described above, into an aqueous hydrazine (Sigma Aldrich) solution for 48 h at ambient temperature. The weight ratio of GO to hydrazine was about 10:7. During the course of reduction, the composite films changed their color appreciably, from dark brown to black. Hydrazine is not known to affect the alginate, therefore the color change indicates the reduction of GO. After reduction, the composite films were washed with demineralized water, dried under vacuum at 50 °C and stored in the desiccator with silica gel as the drying agent. Prior to further analysis, the samples were kept in the furnace at 50 °C under vacuum for at least 48 h.

2.2. Characterization

Thermogravimetric analysis (TGA) was conducted by using a Perkin-Elmer Thermogravimetric Analyzer TGA7 equipped with a Thermal Analysis Controller TAC 7/DX, from 25 to 400 °C (3 °C/min) under air atmosphere.

Electrical conductance of composite samples was measured with a four-point probe device. It consisted of four equally spaced (1 mm) tips of finite radius connected to voltmeter (Keithley 2000) and ammeter (Keithley 6221). A constant voltage of 10 V was applied to the two inner tips, and an ammeter connected to the two outer tips was used to measure current through the sample. Each measurement was repeated 3 times. As the thickness of samples was significantly smaller than the spacing between the tips, the bulk resistivity ρ was obtained by following relation [15]:

$$\rho = Cd\left(\frac{V}{I}\right) \qquad (1)$$

where: d is the thickness of the sample, V – applied voltage, I – measured current and C = 4.523 the cell constant.

The results are presented as the bulk conductivity, which is inverse of the bulk resistivity.

Dynamical mechanical thermal analysis (DMTA) was performed on a DMA Q800 (TA Instruments) instrument in a tensile mode at a frequency of 1 Hz, 5 μm amplitude, and heating rate of 3°C /min. The samples were initially conditioned at 60 °C for 30 min, then cooled and analyzed from 10 – 200 °C.

Creep tests were conducted on a DMA Q800 (TA Instruments) instrument at 30 °C, 40 °C, 60 °C, 80 °C and 100 °C using the same specimen as for DMTA, and applied creep stress of 4 MPa. The duration of the creep and strain recovery was 10 min and 30 min, respectively. The samples were conditioned for 5 min at each temperature before applying the load. The creep

and strain recovery at 30 °C was performed twice for each sample in order to release the resulting stress, that develops during sample preparation.

3. Results

3.1. Thermogravimetric analysis

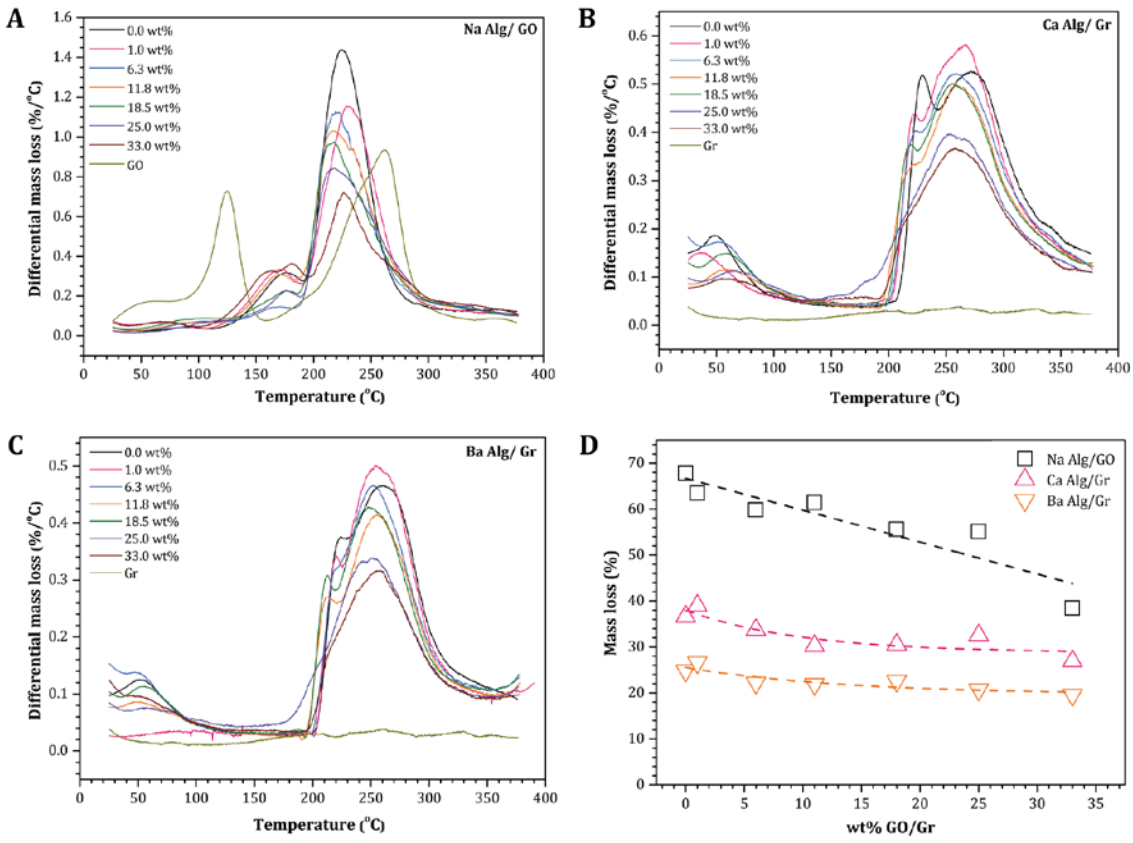

Figure 1. Differential weight loss thermograms of (A) Sodium alginate/graphene oxide (Na-Alg/GO); (B) Calcium alginate/reduced graphene oxide (Ca Alg/Gr), and (C) Barium alginate/reduced graphene oxide (Ba Alg/Gr) composites. Figure (D) gives the total relative relative weight loss dependence on the amount of the filler, taken at the decomposition temperature. Dashed lines serve as guides to the eye only

Figure 1 A-C shows the differential weight loss thermograms collected for three different types of alginate composites with varying weight fraction of filler. The initial weight loss up to 100 °C for all the samples will be due to the elimination of free water as has been found before [16].

Figure 1A represents the differential weight loss thermogram of Sodium alginate and its composites with various weight fractions of graphene oxide (GO). Sodium alginate itself exhibits two significant weight loss peaks at ~173 °C and ~224 °C, corresponding to the loss due to decomposition into volatile components, partially with intermediate dehydration, and the decomposition of polymer into carbonaceous residue [17], respectively. As the concentration of GO increases, the Na Alg weight loss peaks shift to lower temperatures. In addition, at high weight fractions of GO (~30wt%), a new peak gradually develops at ~ 160 °C. Such changes can be explained by the hydrophilic nature of GO, where upon increasing its concentration more moisture has been trapped in the composite, thereby slightly reducing the thermal stability of Na-Alg/GO composites. Neat GO exhibits a sharp decrease in weight at ~123 °C due to the removal of moisture and decomposition of COOH groups [18]. The second weight loss peak ~260 °C can be ascribed to the removal of the remaining labile oxygen groups [19]. In addition, the absence of a weight loss peak at ~120 °C in Na-Alg/GO composites indicates interaction, presumably of a physical origin, between the carboxyl groups of GO and oxygenated groups on the polymer backbone. Indeed, the formation of an extensive hydrogen-bonding network between oxygenated groups of GO and polymer backbone has been investigated by Chen et al. [10b]

Contrary to neat GO, hydrazine reduced GO (rGO) exhibits negligible weight loss in the 25-400 °C range, which is consistent with results reported previously [18-20]. As for Sodium alginate, the thermal degradation of Calcium alginate (Ca Alg) occurs in two steps, with differential weight loss peaks observed at ~230 °C and ~270 °C. The former corresponds to dehydration [21]

and the latter to decomposition of the polymer [22]. As the concentration of rGO in the polymer matrix increases, the thermal stability of the composite films somewhat reduces. This happens presumably due to the remaining hydroxyl groups at the edges of the graphene sheets upon reduction with hydrazine [18] that together with the hydrophilic groups on the alginate backbone can easily bind water molecules, hence reducing the thermal stability of the composite films.

The thermal degradation of Barium alginate also takes place in two steps within the investigated temperature range. Similarly to Calcium alginate, the weight loss peaks are observed at ~226 °C and ~260 °C, and have been ascribed to dehydration and decomposition of the polymer. Also, the peaks tend to lower temperatures upon increasing the concentration of rGO in the Barium alginate matrix.

Figure 1 D illustrates the total weight loss dependence on filler concentration for the various composite systems as obtained at the decomposition temperature. (The decomposition temperature is taken to be the center of the highest temperature peak in the thermogram.) As discussed before, Na-Alg/GO composites exhibit the most significant weight loss in comparison to the alkali earth metal ion cross-linked-rGO composites. Upon inclusion of GO sheets, the weight loss of Sodium alginate composites decreases with a near linear dependence on filler weight fraction. This suggests, that the major mass loss of the composite films occurs due to the decomposition of the polymer only. For instance, the experimentally measured mass loss of Na-Alg/GO with 11.8 wt% of GO is 61.4%, and assuming a constant polymer mass loss as obtained for the pure system, the calculated value is found to be 60.3%. The weight loss of an alkali metal ion cross-linked sample is significantly reduced, and varies only slightly with the concentration of graphene. Also here, the major weight loss originates from the decomposition of the polymer. The reduction in observed mass loss is the result of the cross-linking.

3.2. Electrical conductivity

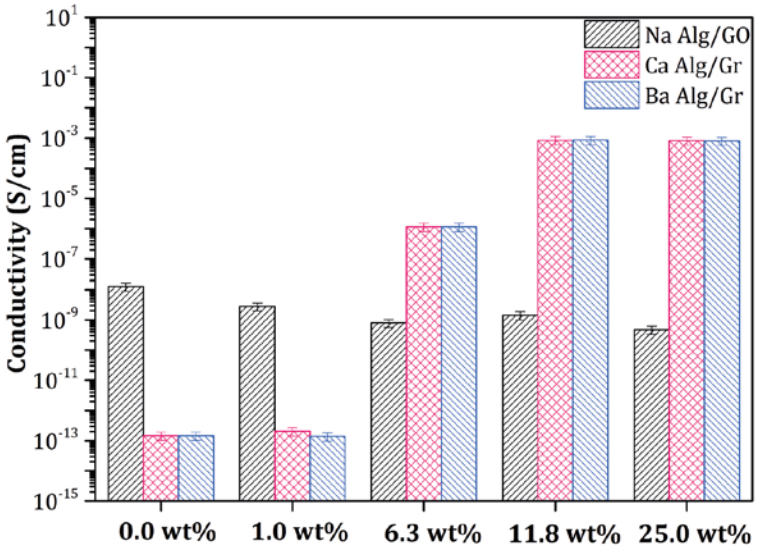

Figure 2. Electrical conductivity of alginate composites versus the weight fraction of filler.

Figure 2 illustrates the electrical conductivity of different alginate composites with various weight fractions of filler. As seen in the graph, the pure alginates are good insulators and their insulating properties further increase upon cross-linking with divalent metal ions and addition of GO. With increasing weight fraction of GO, the electrical conductivity of Na-Alg/GO decreased about 1 order of magnitude compared to neat Sodium alginate due to the good insulating properties of GO [23]. On the other hand, the electrical conductivity significantly improves with reduction of GO. As seen in Figure 2, the electrical conductivity of divalent metal ion cross-linked alginate-rGO composites increases by approximately 10 orders of magnitude and levels off beyond 12 wt% of rGO. However, it still remains several orders of magnitude lower than previously reported for other composite systems, even with much lower weight fractions of filler [24]. Although, it has been proposed that cross-linking alginate with Calcium facilitates distribution of graphite into hydrogel matrix thereby promoting electrical conductivity [25], our results suggest that divalent metal ion-polymer, divalent metal ion-rGO, and rGO-divalent metal ion-polymer interactions, preclude the formation of a connected

graphene network that is required to establish effective conductive paths as explained by the classical percolation theory [26]. We further discuss filler-polymer interactions in the Discussion section.

3.3. Mechanical properties

Figure 3 A-C shows DMTA results obtained for various types of alginate films with varying concentrations of filler. Figure 3 D summarizes the filler concentration dependence of the storage modulus for the three composite systems at the temperature of 30 °C. Even without addition of filler, the neat polymers exhibit remarkably high storage modulus values that agree with values previously reported for Sodium alginate [27] and Calcium alginate [13]. As the amount of GO in the Sodium alginate composite increases, so does the storage modulus, a trend also observed by other authors [10a, 10b]. Alkali earth metal ion cross-linked alginates and their composites exhibit more dramatic changes in storage modulus values for different weight fractions of graphene. Upon inclusion of rGO, the stiffness of Calcium alginate composites initially decreases significantly only to recover and reach a maximum stiffness at 11.80 wt % of rGO, albeit still lower than that of the neat polymer. Conversely, Ba-Alg/GO composites with increasing graphene content show improved stiffness, which decreases beyond 18.50 wt% of rGO.

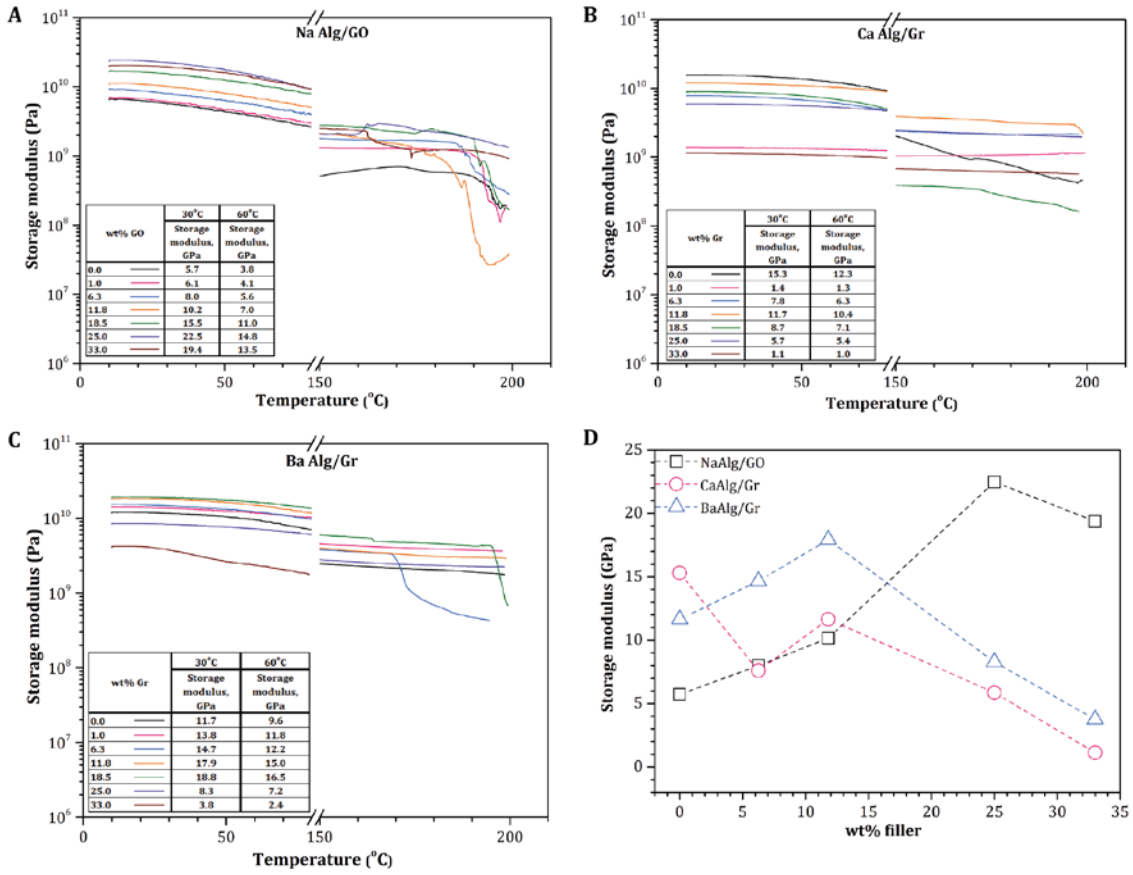

Figure 3. Storage modulus values for composite films of (A) Na-Alg/GO, (B), Ca-Alg/GO, (C) Ba-Alg/GO and (D) its dependence on filler concentration for various types of alginates at 30 °C. Dashed lines serve as guides to the eye only.

In addition, we have attempted to determine the glass transition temperature T_g of the different alginate composite systems using the loss modulus as obtained from DMTA measurements and presented in Figure 4. Unfortunately, due the absence of a well-defined loss modulus peak for Sodium alginate and its composites, we have not been able to accurately determine the glass transition temperature. We point out that all our composite systems contain ~30wt% glycerol as a plasticizer, which substantially reduces the molecular friction between Sodium alginate chains. For the Sodium alginates composites, this probably shifts the T_g values to a temperature out of the experimental window. Barium and Calcium

alginate composite systems, however, are cross-linked and therefore yield distinct loss modulus peaks as seen in Figure 4 A-B.

Figure 4 C-D illustrates the glass transition temperatures of different families of cross-linked alginates. They exhibit varying dependence on the amount of graphene. With increasing amount of filler, the T_g for Ca-Alg/GO composites slightly increases, suggesting reduced chain mobility upon inclusion of filler. In contrast, Ba-Alg/GO composites show a relatively constant T_g independent of the amount of graphene, indicating little or no effect on the mobility of the polymer chains.

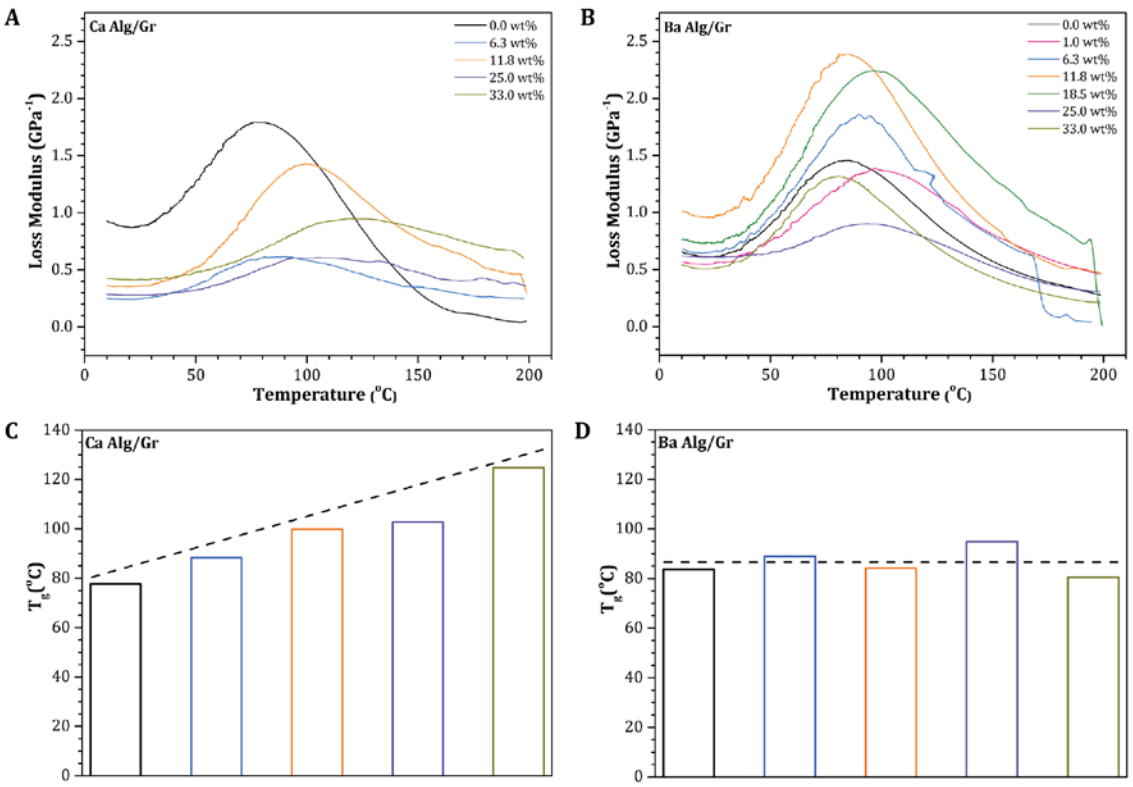

Figure 4. Loss modulus at $1s^{-1}$ versus temperature curves for (A) Ca-Alg/GO and (B) Ba-Alg/GO composites. Glass transition temperatures, as determined from the peak of loss modulus, for various compositions of (C) Ca-Alg/GO and (D) Ba-Alg/GO composites. Different colors

represent different compositions as indicated in the graphs (A) and (B). Dashed lines serve as guides to the eye only.

3.3. Creep test

In order to gain more information about the load performance of the different types of alginates and their composite systems, we have conducted creep tests as described in the experimental part. Figure 5 displays the creep compliance, being the observed strain over the exerted stress, and strain recovery of Na-Alg/GO, Ca-Alg/GO and Ba-Alg/GO composite systems at 60 °C.

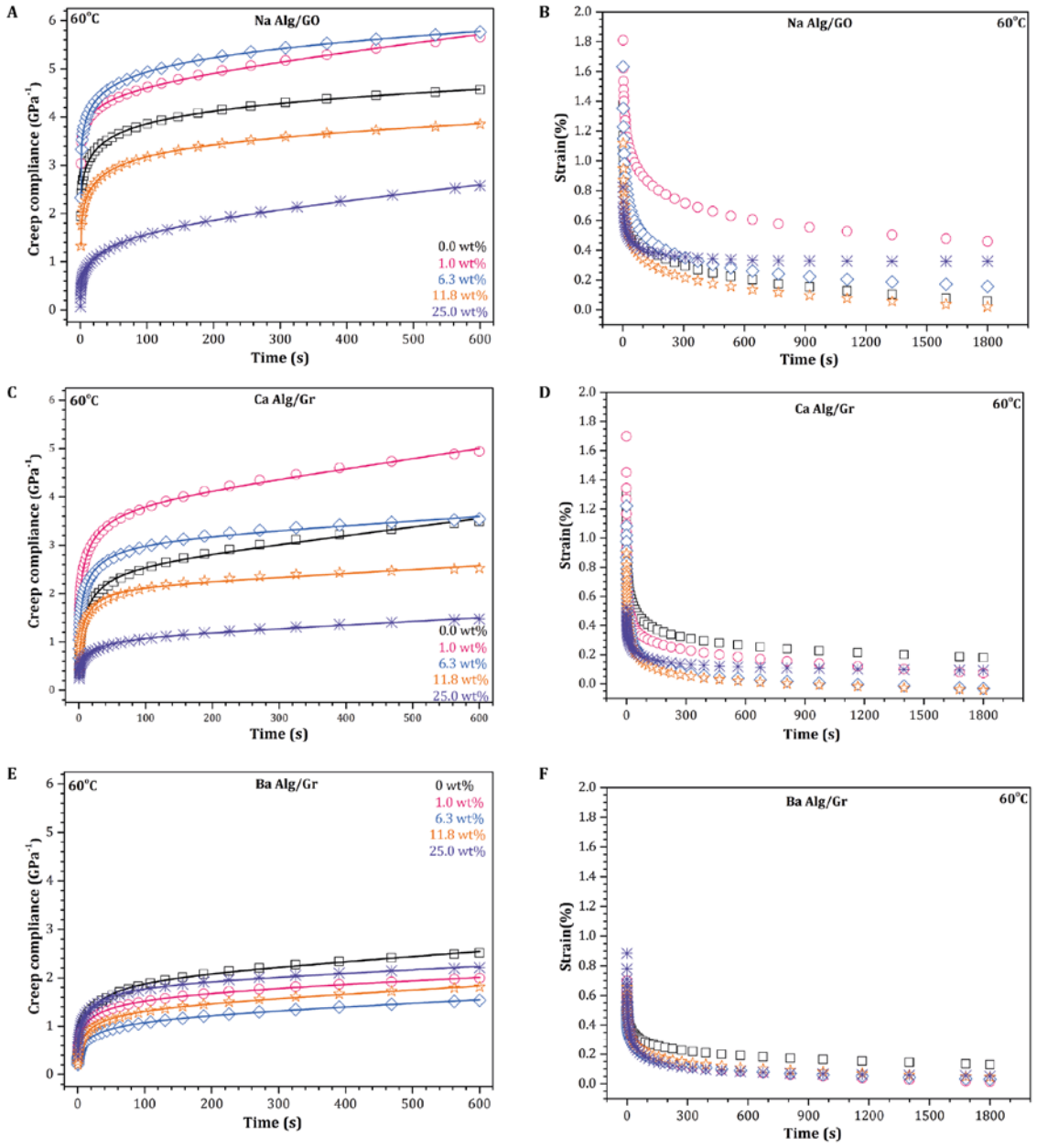

Figure 5. Creep compliance and strain recovery for (A,B) Na-Alg/GO, (C,D) Ca-Alg/GO, and (E,F) Ba-Alg/GO composites. Lines are fits by a modified Burgers' four element model , see text.

Of the three different alginate composite systems, the Na-Alg/GO system reveals the poorest creep resistance. At low (1 wt%) and moderate (~6 wt%) weight fractions of GO, the samples demonstrate lower creep resistance compared to the unfilled polymer. However, the load bearing of Na-Alg/GO composites improves at higher weight fractions, above about 11 wt%, of

filler. Unlike Na-Alg/GO composites, both earth-alkali metal ion cross-linked alginate composites exhibit complex filler weight dependence, see Figure 4 D-F.

Since all creep compliance curves largely exhibit a viscoelastic nature of the samples, we have used Burgers' four-element model to describe the behavior. The model, see Eq. (2), is represented by an elastic element (spring) representing the instantaneous creep and a viscous element (dashpot) to represent the irrecoverable creep, J_0 and J_2 respectively in Eq. (2). This series network is connected to a Kelvin-Voigt element (spring and dashpot in parallel) to represent the actual creep. This creep response is usually more complex than can be described by a simple Kelvin-Voigt system as usually polymers and their composites possess a spectrum of relaxation times [28]. To account for this, we have used a modified Burgers' model, where the exponential term, with coefficient J_1, is replaced by a stretched exponential term with an exponent n to account for the dispersion. The same model has successfully been used to accurately describe creep compliance of the polyimide PMR-15 [29] and bismaleimide-clay nanocomposites [30]. Hence, the creep compliance $J(t)$ as a function of time t can be expressed as

$$J(t) = J_0 + J_1\left[1 - \exp\left(-\left(\frac{t}{\tau}\right)^n\right)\right] + J_2 t \qquad (2)$$

We used the storage modulus values derived from the dynamical mechanical thermal analysis at a representative temperature for the instantaneous creep compliance J_0 as this represents the response at small time scales, i.e. at 1 s^{-1}. The irrecoverable compliance J_2 describes the permanent deformation of the sample, on the molecular level regarded as the slip of polymer chains relative to each other, and is expected to have a relative low value. The effective retardation time τ, corresponds to the time required for the macromolecular matrix to rearrange. The stretching exponent n accounts for the distribution of relaxation times and

assumes values between 0 and 1. A value of unity represents a single relaxation time whereas a lower value of *n* indicates a wider distribution of relaxation times [31]. As shown in the Figure 5, the modified Burgers' model can be fit to the data with excellent accuracy using only four free variables. The obtained values for Na-Alg/GO, Ca-Alg/GO and Ba-Alg/GO composite systems at 60 °C are presented in the Table 2.

Table 1 The obtained parameters for the modified Burgers' model for different alginate composite systems at 60 °C, see also Figure 4.

Composition		J_0 (GPa^{-1})	J_1 (GPa^{-1})	τ (s)	n	J_2 ($TPa^{-1}s^{-1}$)
Polymer	**Filler (wt%)**					
Na-Alg/GO	0.0	0.27	4.8	22.7	0.20	0.32
	1.0	0.24	5.1	2.2	0.14	1.50
	6.3	0.18	6.2	13.7	0.17	0.47
	11.8	0.14	3.7	14.7	0.26	0.48
	25.0	0.07	1.8	35.5	0.39	1.50
Ca-Alg/GO	0.0	0.081	2.5	13.2	0.45	1.60
	1.0	0.76	3.0	9.7	0.44	2.00
	6.3	0.16	2.9	7.6	0.40	0.91
	11.8	0.01	2.1	8.7	0.44	0.67
	25.0	0.19	0.9	16.5	0.47	0.67
Ba-Alg/GO	0.0	0.10	1.8	16.7	0.48	1.10
	1.0	0.09	1.6	15.8	0.36	0.60
	6.3	0.08	1.1	21.8	0.42	0.66
	11.8	0.07	1.3	15.7	0.44	0.80
	25.0	0.14	1.7	11.2	0.43	0.69

Finally, we have attempted to predict the long-term creep behavior of Calcium and Barium alginate-rGO composites at 60°C by applying the time-temperature superposition principle [32], whereby viscoelastic data at one temperature can be transformed to that of a different temperature by shifting it along the time axis. The master curves and shift factors for different families of alginate composites are presented in Figure 6.

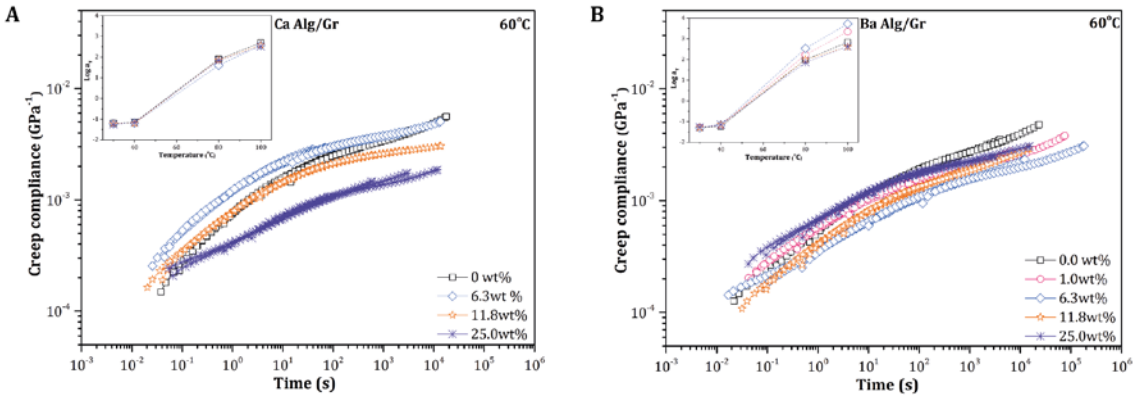

Figure 6. Master curves of creep compliance versus scaled time for (A) Calcium alginate and its composites, and (B) Barium alginate and its composites at 60°C. The insets show the shift factors used in the scaling.

It is apparent that inclusion of rGO sheets improves the long-term creep behavior for both composite systems. Additionally, the slopes of the master curves of the composites are slightly lower, suggesting a small reduction in the creep rates. However, the non-monotonous improvement of the long-term creep compliance illustrates the complexity of the undergoing processes during creep.

4. Discussion

In the following we shall compare the two classes of alginate composites that can be distinguished on whether or not the alginate matrix is cross-linked or not.

4.1. Na-Alg/GO composites

Within the explored temperature regime the thermal stability of the alginate films appears to be largely independent of filler. Changes in mass loss follow the reduction of the amount of polymer only, see Figure 2D and the associated discussion. A notable observation, though, is the disappearance of the GO mass loss due to dehydration, around 120 °C as shown in Figure 2A, which does signify hydrogen-bonding based interactions between oxygenated groups of

GO and alginate. Electrical conductivity of Na-Alg/GO composites, on the other hand, exhibits some filler concentration dependence. The level of insulation of the composites slightly improves at higher weight fractions of GO.

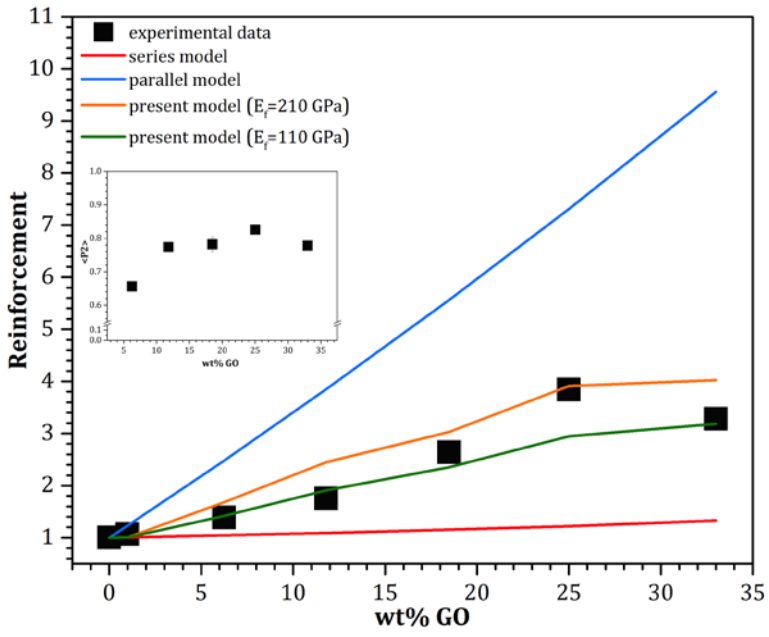

Figure 7. Predicted and measured reinforcement of Na Alg by GO as a function of filler weight fraction. The inset shows the order parameter $\langle P_2 \rangle$ as a function of GO concentration. The reinforcement is taken to be the elasticity of the composite material relative to the elasticity of the polymer matrix (data from Fig. 3 D).

Likewise, the reinforcement, i.e. the elasticity ratio E_c/E_m of composite material relative to its polymer, of the Sodium alginate matrix by introduction of GO sheets indicates moderate interactions between filler and polymer as the reinforcement varies with the filler amount, see Figure 3D. In order to quantify this effect we have invoked the Takayanagi models as discussed in detail by Sperling [7]. The original model has been derived to estimate the stiffness of multiphase polymers such as polymer blends. It has been demonstrated earlier that the model also adequately describes polymer composite materials [33]. In the latter case, the mechanical response of the composite depends on the stiffness of the polymer matrix, E_m, and of the filler,

E_f, as well as on its volume fraction, ϕ_f. We argue that the orientation of the GO sheets in the polymer matrix also matters. In the present experiments, the deformation takes place in the length direction of the film, perpendicular to the film normal. In the case of randomly oriented GO sheets in the Sodium alginate matrix, the stress transfer from the polymer matrix to the GO sheets upon deformation perpendicular to the layer normal of the sample will be inadequate, resulting in the lowest possible reinforcing effect, represented by the series model, Eq. 3, and graphically shown in Figure 7 (red line). On the other hand, the load transfer in a composite with perfectly aligned GO sheets will be optimal, yielding the highest reinforcing effect; shown as the parallel model, Eq. 4, in Figure 7 (blue line). These two cases cannot accurately describe the actual reinforcement for partially aligned filler but rather serve as extremes.

$$E_{\perp} = \left[\frac{\phi_f}{E_f} + \frac{\left(1-\phi_f\right)}{E_m} \right]^{-1} \quad (3) \qquad \text{(Series model)}$$

$$E_{II} = \phi_f E_f + \left(1-\phi_f\right) E_m \quad (4) \qquad \text{(Parallel model)}$$

$$E_c = \left[\frac{\langle P_2 \rangle}{E_{II}} + \frac{\left(1-\langle P_2 \rangle\right)}{E_{\perp}} \right]^{-1} \quad (5) \qquad \text{(Present model)}$$

We have recently reported [34] that GO sheets show high orientational order in the Sodium alginate matrix, that would undoubtedly influence the composite stiffness in the axial direction. Therefore we have attempted to fit our data with a mechanical model that provides the relation between the stiffness of the polymer matrix and composite material, and depends on the average orientational order of GO sheets inside the polymer matrix, shown as the curves labeled “present model” in Figure 7. The inset shows the measured order parameter values, $\langle P_2 \rangle$, as a function of GO concentration. The stiffness of the composite material was

estimated by using Equation 5, a similar expression was originally derived to predict stiffness of a highly oriented aramid fiber [35]. As can be seen in Figure 7 (yellow and green lines), the model adequately describes the reinforcing effect of oriented GO sheets inside the Sodium alginate matrix taking into account the variation of order parameter. The stiffening effect is present up to 25wt% of GO, beyond which both the reinforcement and the order begin to decrease due to jamming effects of neighboring GO sheets. In addition, the reinforcement also depends on the stiffness of GO sheet, which we have taken to be 210 GPa [36]. However, it is not unreasonable to assume that harsh graphite oxidation reaction conditions can produce defects, such as holes, inside GO sheets, that, in turn, influence the stiffness of GO sheets. In addition, the stress transfer of multilayered GO sheets is expected to be inferior to mono/bi-layer GO due to sliding of the sheets past each other, as has been reported to be the case for graphene – polymer nanocomposites [37]. Therefore, we included the curve for a GO stiffness of 110 GPa, which provides a lower bound for the measured reinforcement values.

The inferior creep resistance of the samples containing low and moderate weight fractions of GO, see Figure 5 A-B, can be explained by the slight stacking of GO sheets and weakness of the network formed by the GO sheets due to the consequently larger distance between the stacks than what could be realized by homogenously distributed sheets. As such, it supports the hypothesis of relatively strong hydrogen bonding based polymer-filler interactions. In order to estimate the average stack size, we used our previously calculated interlayer distance between GO sheets for various compositions of Na-Alg/GO composites [34]. The average GO stack size is found using the Scherrer equation [38]. This number is subsequently divided by the interlayer spacing of GO to yield the average number *N* of GO sheets per stack. As seen in Figure 8 A, there are already agglomerates at low weight fractions of sheets. We note, however, that assessment of the average GO stack size at greater weight fractions of the filler can be less accurate due to the lateral inclusion of the sheets, which broadens, and sometimes skews, the

diffraction peak, therefore reducing the obtained average number of sheets per stack. As presented in Figure 8 A, *N* tends to higher values with increasing weight fraction of GO, however does not do so monotonously for reasons discussed earlier. At higher filler weight fractions, the stress distribution improves due to the formation of a network between GO aggregates that compensates for the effect of further increment of *N*.

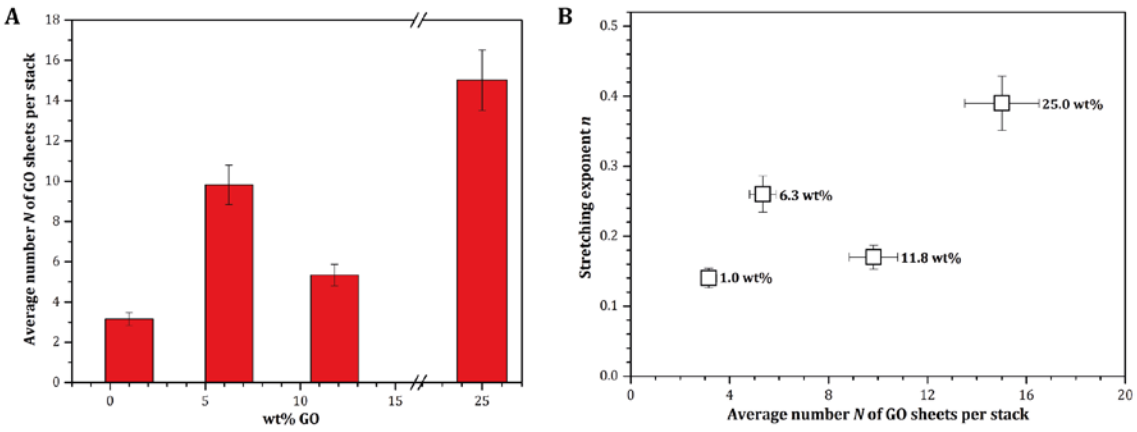

Figure 8. (A) Average number, *N,* of GO sheets per stack depending on the weight fraction of the filler. (B) Stretching exponent versus average number *N* of GO sheets per stack.

The behavior of the creep resistance in Figure 5 A-B is reflected by the parameter values obtained from a fit with the modified Burgers' model, see Table 1. For instance, with increasing GO concentration the creep retardation time τ initially sharply decreases to slowly increase with filler concentration. At 25 wt% of filler it exceeds that of the neat polymer. The stretching exponent *n* shows the same trend, initially it diminishes to increase at higher weight fractions of GO. The same tendency is also present in the creep compliance, J_1, values. Such consistent variation of parameters suggests that at low weight fractions of GO, the polymer chains gain more mobility due to the introduction of the sheets and the frailty of their network that does not build up to expectation due to stacking. Upon further increment of the filler concentration, the mobility of the chains begins to decrease due to the higher concentration of

aggregates, forming a robust network. As shown in Figure 8B, it appears that the stretching exponent *n* depends on the average number *N* of GO sheets in a stack. It increases with increasing *N*, indicating that the distribution of relaxation times is reduced upon strong introduction of GO sheets that reduces polymer chain mobility. Indeed, the formation of a hydrogen-bonding network between oxygenated groups of the polymer and GO sheets further decreases polymer chain mobility.

In summary, the thermomechanical behavior of Na-Alg/GO composites can be understood from the modification of the polymer-polymer interactions by introduction of the polymer-filler interactions. Our data suggests that after oxidation, graphene sheets possess high surface energy that results in strong filler-filler interactions that lead to incomplete dispersion of GO sheets. On the other hand, the plentiful of oxygenated groups on alginate chains and GO sheets ensures the formation of extensive hydrogen-bonding network that is strong enough to fully integrate the filler aggregates into the polymer.

4.2. Alkali metal cross-linked alginate films

Where for Na-Alg/GO composites there are only three kinds of interactions to consider, namely filler-filler, polymer-polymer and polymer-filler, the situation for cross-linked alginate-rGO complexes is much more involved. We will argue that for the cross-linked films the observed changes in stiffness and glass transition temperature are caused by competing reactions between the polymer, the sp^2 clusters and carboxyl groups of the graphene sheets and the alkali earth metal ion during the ion exchange reaction of Na-Alg/GO films. First of all, it has been reported that different multivalent metal ions exhibit different affinity to the alginate matrix [39], namely that Barium ions associate easier with the oxygenated groups on the alginate backbone than Calcium ions do. Indeed, Fourier Transform Infrared Spectroscopy of divalent metal ion cross-linked alginates revealed more specific interactions with Barium ions

compared to Calcium ions [40]. In addition, it has been shown that different divalent metal ions binds have prefential binding sites to the oxygenated groups of alginate such as that Barium ions preferentially associate with guluronic-guluronic acid and mannuronic-mannuronic acid blocks, whereas Calcium – to guluronic-guluronic and mannuronic-guluronic acid blocks [41]. However, it appears that the bonds between divalent metal ions and oxygenated groups of alginates are of dynamic origin as they undergo bond breakage and reformation even under small stress [42]. Secondly, both Barium and Calcium ions interact with sp^2 clusters on reduced graphene oxide sheets via cation – π interactions as discussed by Sun et al. [43]. The authors of this study have shown that metal ions intercalate between graphene sheets, bind to them at different positions with a binding energy that is higher for Barium ions than for Calcium ions. Furthermore, it has been reported that divalent metal ions can also bridge between adjacent GO sheets [44]. We would like to reiterate that we conduct the ion exchange reaction of Na-Alg/GO composites with divalent metal ion salt solutions, and subsequently reduce the metal ion cross-linked/GO composite films in the aqueous hydrazine solution. Thus, it is highly likely that divalent metal ions also form rGO-metal ion-polymer junctions together with rGO-metal ion-rGO interactions. As reduction of GO with hydrazine only eliminate epoxy and hydroxyl groups [45], the carboxyl groups remain unaffected, and hence the connections between graphene sheets, divalent metal ions and polymer backbone persist as manifested in the insolubility of cross-linked composite samples.

Based on the above information and experimental evidence, we argue that the higher affinity of Barium ions for the polymer and filler sheets improves the stress distribution in the Ba-Alg/GO composites as manifested by the higher storage modulus values in comparison with Ca-Alg/GO composites. At high weight fractions of filler, however, the load distribution for both composite systems appears to be impaired, presumably due to the jamming effects of filler sheets. X-ray diffraction (XRD) patterns of Ca-Alg/GO composites revealed an amorphous

structure, whereas those of Ba-Alg/GO composites indicated the presence of a semi-crystalline structure and of the formation of incommensurately modulated structures upon inclusion of graphene [34]. As seen in the figure 4C-4D, unfilled Barium alginate possesses higher T_g temperature than Ca Alg, which agrees with XRD data. We, therefore, propose that the semi-crystalline structure of Barium alginate arises due to the preferential binding of Barium ions to mannuronic acid blocks that enable these junctions to attain more linear conformation whereas guluronic acid-Barium junctions retain more folded structure, see the reference [41] for the schematic illustration.

With increasing weight fraction of graphene, however, the alginate chain mobility appears to be reduced in the Ca-Alg/GO composite system, whereas it remains constant for Ba-Alg/GO composites. Such distinctive behavior could be attributed to the different interactions between the constituents of the composites. We suggest that in Ca-Alg/GO composites there are more Calcium mediated polymer-rGO junctions, which grow in number with increasing amount of filler, than there are Calcium mediated polymer-polymer junctions as well as rGO-rGO junctions, thus reducing polymer chain mobility. On the other hand, in the Ba-Alg/GO composite family it appears to be more separate rGO-Ba^{2+}-rGO and polymer-Ba^{2+}-polymer junctions that result in the development of a two-phase system with increasing amount of rGO. Such an interpretation agrees with our experimental finding of the development of a periodic structure as observed in XRD experiments, measured electrical conductivity, and of the invariability of T_g. Indeed, the presence of divalent ions in the discussed structural arrangements of divalent metal ion cross-linked-rGO composites should be responsible for the high percolation threshold and mediocre electrical conductivity properties of the composite films.

The non-monotonous behavior of creep compliance and strain recovery for the cross-linked alginate composites as illustrated in Figures 5C-5F, manifests the complexity of interactions between the constituents. As mentioned earlier, ionically cross-linked divalent metal alginate junctions undergo ionic bond breakage and reformation under stress [42]. This partial de-cross-linking of an ionically cross-linked junction begins at low stress levels, efficiently dissipating the force. Subsequent increase in the stress, initiates partial de-cross-linking of a neighboring junction, in this way preventing from complete collapse of cross-linked blocks. Our findings suggest that both Calcium and Barium alginates dissipate deformation energy in a similar manner, albeit that Barium alginate possesses slightly better creep resistance that can be attributed to the higher affinity of Barium ions as discussed above. However, stress relaxation mechanisms of divalent metal ion cross-linked alginates-rGO composites are more intricate. As introduced earlier, the bridging of GO sheets with divalent metal ions lead to the enhancement of mechanical properties [44]. Upon bridging two adjacent GO sheets in-plane, the resistance to deformation along the layer normal has been shown to improve. On the other hand, if divalent metal ions both bridge adjacent GO sheets and are intercalated between them, the deformation mechanism has been reported to become more complicated, and metal ion size-dependent. Since in our experimental procedure we do not have control over binding sites of divalent metal ions, their interaction with polymer chains and, especially, with GO sheets, can result in variety of possible structural arrangements that, in turn, seem to result in difficult-to-predict trends in the creep compliance curves.

The complexity of stress relaxation mechanisms in divalent metal ion cross-linked alginates and their composites is reflected in the fit parameters presented in Table 2. For both the metal ion cross-linked systems, the stretch exponent increases, indicating a narrower distribution of relaxation times, as a result of cross-links. In addition to this, the retardation time τ for various compositions of metal ion cross-linked alginates increases in comparison with Sodium alginate

composites. Furthermore, depressed creep compliance J_1 values corroborate reduced polymer chain mobility. However, both alkali earth metal ion cross-linked alginates show a complicated rGO concentration dependence indicating complex interactions that may be difficult to decouple.

In effect, introduction of divalent metal cations in alginate – rGO composites significantly alters polymer – polymer, polymer – filler, and filler – filler interactions. Our data shows that these interactions are strongly influenced by the affinity of metal ions to oxygenated groups of alginate chains as well as filler sheets. Depending on the nature of the metal cation and the filler weight fraction, the interactions between the polymer and filler can be rendered to be stronger as in the case of Ba-Alg/GO composites, or weaker as for Ca-Alg/GO composites. However, in order to determine the precise interactions between the constituents of divalent metal ion cross-linked alginate-graphene composites, our present data is insufficient, and a more detailed study wil be required.

5. Conclusions

We have investigated thermal, electrical and mechanical properties of graphene (oxide) – alginate biopolymer nanocomposites and have shown these to be composition dependent. Thermogravimetric data analysis revealed favorable interactions between GO and Sodium alginate polymer chains. However, thermal stability of Na-Alg/GO composites showed no dependence of the filler weight fraction, and was slightly inferior to that of the unfilled polymer due to the hygroscopic nature GO sheets. On the other hand, upon introduction of cross-linking junctions in alginate – graphene nanocomposites thermal stability was improved, though not influenced by the presence of rGO sheets.

On the other hand, the electrical properties appeared to be composition dependent. Whereas electrical conductivity of Na-Alg/GO composites decreased with increasing amount of GO, the

electrical conductivity of divalent metal ion cross-linked alginate-rGO composites improved about 10 orders of magnitude. However, the measured values remained several orders of magnitude lower than of other rGO-polymer composites due to the ineffective formation of a percolated conductive network of filler particles.

Similarly, the mechanical properties and the glass transition temperature of alginate – graphene (oxide) nanocomposites are strongly affected by composition in particular the weight fraction of filler. The favorable interactions between GO and Sodium alginate polymer chains as well as orientational order of the filler particles manifests itself in a dramatic increase of the storage modulus of the composites. In addition, the reinforcing effect of GO was modeled by taking into account the orientational order of sheets and yielded accurate description of the experimental data. On the other hand, the properties of alkali earth metal ion cross-linked alginate – rGO nanocomposites were strongly influenced by the divalent metal ion. Our experimental results show the formation of dissimilar microscopic structures that in a complex way influence the electrical conductivity, the elasticity of the nanocomposites, and the mobility of the polymer chains, which we believe is due to the specific interactions between polymer chains, filler sheets and metal cations. The lack of clear trends in the creep compliance data of different alginate nanocomposites indicates complex stress relaxation mechanisms. Nevertheless, the modified stretched exponential Burgers' model can describe the short-term creep compliance of alginate – graphene (oxide) composites with remarkable precision.

Our study clearly indicates that graphene (oxide) filled alginates form an extremely versatile class of composites that can be tuned at will from hydrophilic to hydrophobic with concurrent variation in electrical conductivity, thermomechanical strength and elastic properties. Many of these phenomena, such as its hydrophobicity, can be understood from relatively simple

considerations whereas others, such as the elastic response, still remain elusive largely due to the intricate interplay between filler-alginate -multivalent ion interactions.

Acknowledgements

This work is supported by NanoNextNL, a micro and nanotechnology consortium of the Government of the Netherlands and 130 partners. The authors also acknowledge dr. M. R. Hegde and B. Norder for fruitful discussions, as well as P.J. Droppert for the assistance with four point probe measurements, and H. Broekhuizen – with the DMA instrument.

References

1. Du, Y.; Shen, S. Z.; Cai, K. F.; Casey, P. S. *Prog Polym Sci* **2012,** *37* (6), 820-841.

2. Kango, S.; Kalia, S.; Celli, A.; Njuguna, J.; Habibi, Y.; Kumar, R. *Prog Polym Sci* **2013,** *38* (8), 1232-1261.

3. Choudalakis, G.; Gotsis, A. D. *Eur Polym J* **2009,** *45* (4), 967-984.

4. Roy, N.; Sengupta, R.; Bhowmick, A. K. *Prog Polym Sci* **2012,** *37* (6), 781-819.

5. Huang, Y. Y.; Terentjev, E. M. *Polymers-Basel* **2012,** *4* (1), 275-295.

6. Huang, X.; Qi, X. Y.; Boey, F.; Zhang, H. *Chem Soc Rev* **2012,** *41* (2), 666-686.

7. Sperling, L. H., *Introduction to Physical Polymer Science*. 4th ed.; John Wiley & Sons, Inc.: 2006; p 880.

8. Ganesan, V. *J Polym Sci Pol Phys* **2008,** *46* (24), 2666-2671.

9. Kuila, T.; Bose, S.; Mishra, A. K.; Khanra, P.; Kim, N. H.; Lee, J. H. *Prog Mater Sci* **2012,** *57* (7), 1061-1105.

10. (a) Ionita, M.; Pandele, M. A.; Iovu, H. *Carbohyd Polym* **2013,** *94* (1), 339-344; (b) Chen, K.; Shi, B.; Yue, Y. H.; Qi, J. J.; Guo, L. *Acs Nano* **2015,** *9* (8), 8165-8175; (c) Cao, K. T.; Jiang, Z. Y.; Zhao, J.; Zhao, C. H.; Gao, C. Y.; Pan, F. S.; Wang, B. Y.; Cao, X. Z.; Yang, J. *J Membrane Sci* **2014,** *469*, 272-283.

11. Grant, G. T.; Morris, E. R.; Rees, D. A.; Smith, P. J. C.; Thom, D. *FEBS Letters* **1973,** *32* (1), 195-198.

12. Pawar, S. N.; Edgar, K. J. *Biomaterials* **2012,** *33* (11), 3279-3305.

13. Russo, R.; Malinconico, M.; Santagata, G. *Biomacromolecules* **2007,** *8* (10), 3193-3197.

14. Kovtyukhova, N. I.; Ollivier, P. J.; Martin, B. R.; Mallouk, T. E.; Chizhik, S. A.; Buzaneva, E. V.; Gorchinskiy, A. D. *Chem Mater* **1999,** *11* (3), 771-778.

15. Smits, F. M. *Bell System Technical Journal* **1958,** *37* (3), 711-718.

16. Hatakeyama, T.; Hatakeyamaa, H.; Nakamurab, K. *Thermochimica Acta* **1995,** *252*, 137–148.

17. (a) Soares, J. P.; Santos, J. E.; Chierice, G. O.; Cavalheiro, G. O. *Eclética Quimíca* **2004,** *29* (2), 53-56; (b) Swamy, T. M. M.; Ramaraj, B.; Siddaramaiah *J Macromol Sci A* **2010,** *47* (9), 877-881.

18. Pei, S. F.; Cheng, H. M. *Carbon* **2012,** *50* (9), 3210-3228.

19. Park, S.; An, J.; Potts, J. R.; Velamakanni, A.; Murali, S.; Ruoff, R. S. *Carbon* **2011,** *49* (9), 3019-3023.

20. Wu, N.; She, X. L.; Yang, D. J.; Wu, X. F.; Su, F. B.; Chen, Y. F. *J Mater Chem* **2012,** *22* (33), 17254-17261.

21. Zhang, J. J.; Ji, Q.; Wang, F. J.; Tan, L. W.; Xia, Y. Z. *Polym Degrad Stabil* **2012,** *97* (6), 1034-1040.

22. Bekin, S.; Sarmad, S.; Gurkan, K.; Yenici, G.; Keceli, G.; Gurdag, G. *Polym Eng Sci* **2014,** *54* (6), 1372-1382.

23. Gomez-Navarro, C.; Weitz, R. T.; Bittner, A. M.; Scolari, M.; Mews, A.; Burghard, M.; Kern, K. *Nano Lett* **2007,** *7* (11), 3499-3503.

24. (a) Wang, X. L.; Bai, H.; Yao, Z. Y.; Liu, A. R.; Shi, G. Q. *J Mater Chem* **2010,** *20* (41), 9032-9036; (b) Pang, H.; Chen, T.; Zhang, G. M.; Zeng, B. Q.; Li, Z. M. *Mater Lett* **2010,** *64* (20), 2226-2229.

25. Qu, B.; Li, J.-r.; Xiao, H.-n.; He, B.-h.; Qian, L.-y. *Polym Composite* **2015**, n/a-n/a.

26. Stauffer, D., *Introduction to percolation theory*. Taylor & Francis: London ;, 1985.

27. Avella, M.; Di Pace, E.; Immirzi, B.; Impallomeni, G.; Malinconico, M.; Santagata, G. *Carbohyd Polym* **2007,** *69* (3), 503-511.

28. Menard, K. P., *Dynamic Mechanical Analysis: A Practical Introduction*. Second ed.; CRC Press 2008; p 240.

29. Marais, C.; Villoutreix, G. *J Appl Polym Sci* **1998,** *69* (10), 1983-1991.

30. Faraz, M. I.; Besseling, N. A. M.; Korobko, A. V.; Picken, S. J. *Polym Composite* **2015,** *36* (2), 322-329.

31. Dean, G. D.; Broughton, W. *Polym Test* **2007,** *26* (8), 1068-1081.

32. (a) Leaderman, H. Elastic and creep properties of filamentous materials. Massachusetts Institute of Technology, 1941; (b) Tobolsky, A.; Eyring, H. *J Chem Phys* **1943,** *11* (3), 125-134.

33. Gearing, J. W. E.; Stone, M. R. *Polym Composite* **1984,** *5* (4), 312-318.

34. Vilcinskas, K.; Norder, B.; Goubitz, K.; Mulder, F. M.; Koper, G. J. M.; Picken, S. J. *Macromolecules* **2015,** *48* (22), 8323–8330.

35. (a) Picken, S. J.; Vanderzwaag, S.; Northolt, M. G. *Polymer* **1992,** *33* (14), 2998-3006; (b) Northolt, M. G.; van der Hout, R. *Polymer* **1985,** *26* (2), 310-316.

36. Suk, J. W.; Piner, R. D.; An, J.; Ruoff, R. S. *Acs Nano* **2010,** *4* (11), 6557-6564.

37. Gong, L.; Young, R. J.; Kinloch, I. A.; Riaz, I.; Jalil, R.; Novoselov, K. S. *Acs Nano* **2012,** *6* (3), 2086-2095.

38. Scherrer, P. *Göttinger Nachrichten Math. Phys.* **1918**, 98-100.

39. Haug, A.; Smidsrod, O. *Acta Chem Scand* **1970,** *24* (3), 843-&.

40. Vilcinskas, K.; Zlopasa, J.; Jansen, K. M. B.; Mulder, F. M.; Picken, S. J.; Koper, G. J. M. *Macromolecular Materials and Engineering* **2016,** *submitted*.

41. Paredes, J. G. A.; Spasojevic, M.; Faas, M. M.; de Vos, P. *Frontiers in Bioengineering and Biotechnology* **2014,** *2* (26), 1-15.

42. Kong, H. J.; Wong, E.; Mooney, D. J. *Macromolecules* **2003,** *36* (12), 4582-4588.

43. Sun, P. Z.; Zheng, F.; Zhu, M.; Song, Z. G.; Wang, K. L.; Zhong, M. L.; Wu, D. H.; Little, R. B.; Xu, Z. P.; Zhu, H. W. *Acs Nano* **2014,** *8* (1), 850-859.

44. Park, S.; Lee, K. S.; Bozoklu, G.; Cai, W.; Nguyen, S. T.; Ruoff', R. S. *Acs Nano* **2008,** *2* (3), 572-578.

45. Gao, X. F.; Jang, J.; Nagase, S. *J Phys Chem C* **2010,** *114* (2), 832-842.